Viscosity-sensitive membrane dyes as tools to estimate the crystal-line structure of lipid bilayers

Miguel Paez-Perez,[a] Michael R. Dent,[a] Nicholas J. Brooks,[a*] Marina K. Kuimova[a]*

[a]*MSRH, Department of Chemistry, Imperial College London, WoodLane, London, W12 0BZ, UK*

*Corresponding authors, e-mail: m.kuimova@imperial.ac.uk, n.brooks@imperial.ac.uk

ABSTRACT

Lipid membranes are crucial for cellular metabolism, and their correct function has been linked to a tight regulation of their structural and mechanical properties, such as viscosity. Fluorescent probes sensitive to the membrane's environ- are being extensively used to investigate the membrane's properties, yet there is currently a lack of understanding on how the lipid organization impacts the readout from these dyes. Here, we investigate this relationship by simultaneously characterizing the membrane's viscosity and structural properties using a combination of X-Ray diffraction, together with environmentally-sensitive optical membrane probes and fluorescence lifetime imaging microscopy. Our results reveal a phase-dependent connection between the different membrane's structural and mechanical parameters and give insight into the relationship between two widely used membrane probes with the structural descriptors of the lipid bi-layer. Such relationship is believed to dictate the lateral organization of lipid bilayers, including the presence of distinct lipid domains which have been traditionally ascribed to a difference in the membrane thickness of the lipid phases; yet we later demonstrate how such connection is not universal and can disrupted by the presence of line-active molecules. Our results show the capability of membrane dyes to directly report on the membrane's molecular structure – after appropriate calibration – and highlight the need of multiple orthogonal characterization strategies for a proper understanding of the membrane's properties.

INTRODUCTION

Lipid membranes are central in cellular metabolism, and are known to be involved in cellular adaptation, homeostasis and disease.[1] This functionality arises from the complex interplay between lipid molecules, which ultimately determines the membrane tension. Under equilibrium conditions, the bilayer's tension is minimized,[2,3] and ultimately this dictates the membrane's mechanical properties, such as elasticity and viscosity; and structural parameters, including membrane thickness and lipid area.[4] Importantly, minimization of the membrane tension may lead to the lipid segregation into regions with distinct composition and biophysical properties.[5,6] According to the 'lipid raft' hypothesis, these lipid domains have a central role in signal transduction and protein organization, and therefore are of high biological interest.[7,8]

Several methods have been developed to study the membrane's structure. Particularly, the high spatiotemporal resolution, capability of multiplexed labelling and biocompatibility offered by fluorescence-based approaches has turned these techniques into the preferred method to study the lateral organization of biomembranes.[9] Moreover, the use of environmentally sensitive dyes has enabled the study of the local molecular organization around the fluorescent probe at biologically-relevant timescales.[10,11]

The use of these fluorophores, including Laurdan,[12] FlipTR[13,14] or molecular rotors (MRs),[15] has enabled the successful mapping of the membrane's microenvironment,[12,13,16] including the effect of the cytoskeletal scaffold on cellular membranes.[17] However, the photophysical properties of many of these molecules depend on multiple membrane parameters (*e.g.* microviscosity, polarity or temperature) and therefore it is challenging to unequivocally assign a physical descriptor to a given fluorescent readout. In fact, such multiple dependency prevents an accurate understanding of what biophysical property of the lipid bilayer is being measured by these sensors (*e.g.* whether they are sensitive to the lipid-lipid separation, membrane thickness, headgroup size etc.)

Uniquely, the fluorescence readout of BODIPY-based molecular rotors (Fig. 1c) has been shown to be solely dependent on the surrounding microviscosity (η) within physiologically relevant values.[18,19] This has enabled the quantitative measure of diffusion rates in lipid membranes[19,20] and could, potentially, allow to relate the bilayer mechanics to its molecular architecture.

In molecular rotors, the non-radiative decay efficiency is coupled to the degree of intra-molecular rotation. Hence, in less crowded and less viscous environments, non-radiative decay is preferred and therefore MR's fluorescence intensity and lifetime τ decrease, as predicted by the Förster-Hoffmann equation:

$$\tau = z\eta^{\alpha} \tag{1}$$

where z and α are calibration constants which are experimentally determined by measuring the MR lifetime in solutions of known viscosity. Remarkably, fluorescence lifetime is independent of the local probe concentration and instrument setup, and this has allowed the direct quantitative mapping of microviscosity in heterogeneous model[20–22] and cellular[23–25] membranes under different stress conditions.[11,22,26] Therefore, we anticipate the fluorescence lifetime of membrane-embedded BODIPY-based MRs could be used to infer changes in the membrane's structure.

Experimentally, the structure and lateral organization of lipid membranes has been quantitatively probed using small and wide angle X-Ray scattering (SAXS / WAXS).[4] SAXS diffraction patterns are used to elucidate the lipid mesophase and, in the case of lamellar structures, they report on the interlamellar distance, from where the membrane thickness (d_{HH}) can be extracted. On the contrary, WAXS is sensitive to the in-plane membrane organization, and the position of the WAXS peak can be used to estimate the average area occupied by a lipid molecule (APL) within the membrane, Fig. 1a.

When the membranes contain different phases, distinct diffraction peaks appear in the SAXS regions, which arise from the difference in the domain's thickness. However, phase separation could occur between domains with very similar or identical thickness, as expected with the highly dynamic nanosized 'rafts',[27] leading to the loss of multiple resolvable SAXS patterns. Alternatively, domains can also be distinguished by their different APL, which can cause the presence of multiple peaks in the WAXS range. Yet, liquid disordered (L_d) and liquid ordered (L_o) phases (which are thought to occur in nature[27]), are characterized by similar distances between lipid molecules, and they are not easily distinguishable by WAXS.[28]

By using a combination of MRs and XRD, we directly calibrate the fluorescence readout of BODIPY MRs against structural parameters of model lipid membranes. We then explore whether such relation holds true for other bilayer systems, including those displaying phase separation, where hydrophobic height mismatch drives the formation of domains with distinct viscosity. Finally, we challenge this relation by incorporating a line-active molecule, oleic acid, to phase separated membranes and evidence how the presence of this lipid is sufficient to disrupt the structural/mechanical relationship expected in canonical lipid bilayers.

EXPERIMENTAL METHODS

Materials: Lipids 1,2-dioleoyl-sn-glycero-3-phosphocholine (DOPC) and 1,2-dipalmitoyl-sn-glycero-3-phosphocholine (DPPC) were purchased from Avanti Polar Lipids® dissolved in $CHCl_3$ (25mg/mL). Oleic acid (OA) and cholesterol (Chol) were obtained from Sigma Aldrich® and dissolved in $CHCl_3$ to a stock concentration of 50mg/mL. Molecular rotor **BC10** was synthesized in house according to a previously published literature procedure (see ESI from ref[25]). All other reagents were purchased from Sigma Aldrich®, VWR or Across Organic and used without further purification. Solvents for fluorescence studies were of spectrophotometric grade.

Large Unilamellar Vesicle (LUV) formation: LUVs were prepared by extrusion. Shortly, lipids in $CHCl_3$ were mixed with either **BC10** or Laurdan at 0.5%mol and the organic solvent was evaporated off under a nitrogen stream. The resulting dry lipid film was further dried under vacuum for >2h to remove any solvent traces. Subsequently, the film was hydrated with water to a final lipid concentration of 1mM and vortexed to yield a cloudy solution of polydisperse multilamellar vesicles. This mixture was then extruded (above the lipid's melting transition temperature) through a 200nm polycarbonate filter to yield a monodisperse LUV population (average diameter of ~180nm determined by DLS).

Spectroscopic characterization of LUVs: LUVs were diluted 10-fold and placed into quartz cuvettes (10mm path length). Emission spectra of Laurdan-labelled vesicles were acquired using a Horiba Yvon Fluormax 4 fluorimeter after 360nm excitation, from which the Laurdan's general polarization (GP) was calculated as:

$$GP = \frac{I_{435\pm2} - I_{490\pm2}}{I_{435\pm2} + I_{490\pm2}} \quad (2)$$

Time resolved fluorescence decay traces of **BC10** labelled liposomes were acquired using a Horiba Jobin Yvon IBH 5000 F time-correlated single photon counting (TCSPC) instrument. A pulsed 404nm diode (NanoLED) was used to excite **BC10**, and fluorescence was detected at 515nm. Acquisition was stopped after peak counts reached 10.000, and the resulting traces were fitted using DAS® software to the minimum number of decay components (2 for gel-phase membranes, 1 for liquid-phase bilayers), ensuring the fitting metric $\chi^2<2$. The intensity-weighted fluorescence lifetime was defined as:

$$\tau_w = \frac{\sum_{i=1}^{n} \alpha_i \tau_i^2}{\sum_{i=1}^{n} \alpha_i \tau_i} \quad (3)$$

where α_i and τ_i represent the relative amplitude and lifetime of the independent decay components. The measured lifetime was then used to estimate membrane viscosity based on the Förster-Hoffmann with the parameters given by *Hosni et al.*[29]:

$$\log_{10} \tau = 0.4569 \log_{10} \eta - 0.75614 \quad (4)$$

Temperature was controlled with a Peltier cell (fluorimeter, error: ±0.5°C) or a water bath (TCPSC, error: ±1°C) and were left to equilibrate for at least 5 min before each measurement.

X-Ray diffraction experiments: Dry samples of a given lipid mixture (20mg total mass) were hydrated with DI water to 70% w/w and subjected to 15 freeze-thaw cycles to ensure a proper lipid mixing. The sample was then loaded into a 2mm diameter polymer capillary tube and sealed with a rubber stopper. SAXS and WAXS measurements were performed at beamline I22 (Diamond Light

Source, UK).[30] Experimental error for OA experiments was obtained from duplicate, independent measurements. For DOPC and DPPC temperature gradients, we ensured sample reproducibility by measuring three independent replicates of the given lipid composition at room temperature.

Giant Unilamellar Vesicle (GUV) formation: Around 30 µL of a 1mg/mL (total lipid, at the desired DOPC:OA:DPPC:Chol ratio and supplemented with 0.5%mol **BC10** or Laurdan) was spread onto an ITO slide to create a thin lipid film. $CHCl_3$ traces were removed by drying overnight in a desiccator. A polydimethyl siloxane (PDMS) spacer with a thickness of ~2mm was then placed on top of the ITO slide to create a chamber, which was then filled with a 0.4M sucrose solution and then sealed using a second ITO slide. GUVs were electroformed (at 60°C) by applying an electric field of $1V_{pp}$@10Hz for 90' followed by a detachment phase of $1V_{pp}$@2Hz for 30'. Finally, GUVs were gently recovered by tilting the chamber (avoiding pipetting in the process).

Confocal Laser Scanning Microscopy (CLSM): Microscopy images were obtained with a Leica SP5 II inverted confocal microscope using a 20x (NA:0.7) dry objective. A Ti:Sapphire laser (Coherent, Chameleon Vission II 80MHz) provided two-photon excitation (900nm), and fluorescence emission was collected either between 425-465nm and 480-520nm. Laurdan's General Polarization (GP) was calculated as:

$$GP = \frac{I_{425-465} - I_{480-520}}{I_{425-465} + I_{480-520}} \quad (5)$$

Fluorescence Lifetime Imaging Microscopy (FLIM): FLIM micrographs were obtained with a Leica SP5 II inverted confocal microscope using a 20x (NA:0.7) dry objective. The Ti:Sapphire laser (Coherent, Chameleon Vission II 80MHz) provided two-photon excitation (930nm), and **BC10** fluorescence emission was collected between 500-580nm. The FLIM images were acquired using a TCSPC card (Becker & Hickl GmbH®, SPC-830). Instrument response function (IRF) was obtained using the second harmonic generation signal from urea crystals. Pixel-wise fitting of the fluorescence decays (Fig. S9) was done by fitting the decays to a monoexponential model (minimum of 200 counts/pixel after binning) using the commercially available software SPCImage®. **BC10** lifetimes obtained with SPCImage® or a custom-written script (see ESI) were transformed to viscosity values according to Eq. 4.

Statistical analysis and data representation: Scatter plots display the mean±S.D. Box plots display the 25–75% range, error bars represent ±S.D., median is shown by a horizontal line and mean by a dot. Origin® software was used to perform one-way ANOVA test. *$p < 0.05$; **$p < 0.01$; ***$p < 0.001$. For the temperature scans, solid lines represent the values obtained by linear fitting of the experimental data (dots) presented in the graph. The shadowed area corresponds to the 95%CI of the linear fit.

RESULTS AND DISCUSSION

Membrane microviscosity correlates with the structural parameters of the lipid bilayer: Initially we explored the relationship between the bilayer's structure, measured by SAXS/WAXS, and its microviscosity, measured by molecular rotor BC10, by systematically increasing the temperature. The gain in thermal energy leads to an increased motion of the lipid's alkyl chains, and this would increase the area per lipid, and decrease the membrane thickness and microviscosity.

Measurements performed on 1,2-dioleoyl-sn-glycero-3-phosphocholine (DOPC) membranes confirmed this trend (Fig. 1b and Fig. 2b-e). This lipid remains in the fluid lamellar phase (L_α)

throughout the chosen temperature range owing to its two unsaturated chains, and its behavior has been studied extensively, hence we selected DOPC as a "gold standard". We observed that heating DOPC membranes from 5 to 65 °C, caused a gradual decrease in membrane thickness, d_{HH}, from 40.7±0.2 to 37.6±0.2 Å and increase in APL from 67.1±0.5 to 73.5±0.5 $Å^2$ (Fig. 2b-e, Fig. S1,S2). These changes are linear with a slope of $(-4\pm0.2)\times10^{-2}$ Å/°C and $(10\pm0.5)\times10^{-2}$ $Å^2$/°C respectively, consistent with previous results for fluid membranes.[31,32] These variations were accompanied by a decrease in the membrane microviscosity (Fig. S2,S3a) from ~420 to ~10 cP. Notably, the change in DOPC viscosity with temperature followed the log-inverse relation described by Andrade's model (Eq. 6, Fig 1d), which suggest DOPC bilayers exhibit a behavior analogous to an ideal liquid.

$$\eta(T) = Aexp\left(\frac{B}{T}\right) \tag{6}$$

We also observed a negative correlation between d_{HH} and APL (Fig. 2c), corresponding to a positive Poisson ratio (ν) typical of bilayers in the fluid phase, where they become thinner as they stretch, in agreement with previous simulations.[33]

Next, we replaced BC10 with Laurdan to investigate whether the commercially available probe displayed similar sensitivity to changes in the membrane structure. In this case, the environmental sensitivity of Laurdan comes from the presence of a dipole moment along its naphthalene moiety, which ultimately leads to a reorientation of the solvent molecules around the dye and to a red shift of the emission spectra in polar/hydrated environments.[34] Therefore, changes in lipid order and membrane hydration will cause a spectral shift of Laurdan spectra.[12] Such alteration is commonly quantified using the general polarization (GP) function (Eq. 5), although some other more advanced spectroscopic approaches have been developed.[35,36]

Increasing temperature resulted in a redshift of Laurdan's fluorescence emission in DOPC membranes (Fig. S3c). However, there was a lack of linear relationship between the response of Laurdan's GP and membrane viscosity reported by BC10 (Fig. S4a) at increasing temperature, suggesting these dyes sense different membrane properties. Therefore, Laurdan response cannot be directly related to the bilayer's structure; and this prevents its use as a tool for quantification of the membrane's properties.

After demonstrating the ability of MRs to report on the molecular structure of simple, fluid membranes we investigated whether such capability is retained in bilayers displaying a more complex phase behavior, such as 1,2-dipalmitoyl-sn-glycero-3-phosphocholine (DPPC). The fully saturated DPPC lipids experience stronger inter-molecular attractive forces, and this significantly decreases DPPC in-plane motion, causing the membrane to be arranged in a highly ordered tilted gel ($L_{\beta'}$) phase. As temperature is increased, the attractive interactions become weaker and the gel membrane transitions towards a ripple ($P_{\beta'}$) phase and, finally to the L_α phase at T>41°C, analogous to DOPC membranes.

At room temperature, DPPC L_β' phase, is evidenced by the two peaks observed in the WAXS pattern (Fig. S5b). Upon heating, an increase of both d_{HH} and APL was observed, Fig. 2g,h ,suggesting a negative Poisson ratio, ν = $(-9\pm0.1)\times10^{-2}$. This behavior can be attributed to a decrease of the lipid tilt, which outweighs the reduction in length of the hydrocarbon chains due to the increase in chain motion (Fig. S2b),[37] and results in both higher membrane thickness and APL with increased temperature. Moreover, the stronger lipid-lipid interactions of gel membranes are also reflected in the higher dependency of membrane viscosity on d_{HH} and APL of gel phases (Fig. 2i,j, blue) compared to DPPC bilayers in the L_α phase (Fig. 2i,j, red), consistent with lack of stress buffering capacity provided by the greater structural flexibility of fluid membranes.

Overall, these results show that, if the response of an environmentally sensitive membrane probe is known and unequivocal, it would be possible to relate the fluorescent readout to the molecular architecture of lipid membranes. Such relation has the potential of being used to infer alterations in the membrane's structure which are not measurable *in-cellulo* using available techniques, such as XRD.

Structure-viscosity relationship is maintained for membranes in the same phase regardless of lipid composition: After measuring the relationship between the structure and microviscosity of DOPC and DPPC membranes, we explored whether such relation could be exploited to infer the structural properties of lipid bilayers with different composition. Given the linear relationship between temperature and the XRD derived parameter $\mathcal{P}$ (either d_{HH} or APL) of the form:

$$\mathcal{P}(T) = \mathcal{P}_0 + b\mathrm{T} \tag{7}$$

where $\mathcal{P}_0$ is the structural parameter at 0K and b is the thermal coefficient; it is then possible to combine Eq. 6 and Eq. 7 to yield:

$$\mathcal{P}(\eta) = \mathcal{P}_0 + \left(\frac{bB}{\ln(\eta) - \ln(A)}\right) \tag{8}$$

To test this hypothesis, we focused on the APL as a structural descriptor instead of d_{HH}, as the former had a greater dependency on viscosity. First, the parameters from Eq. 8 where obtained from the APL and microviscosity obtained for DOPC membranes. Subsequently, we employed BC10 to measure the microviscosity of 1-palmitoyl-2-oleoyl-glycero-3-phosphocholine (POPC) and 1,2-dilauroyl-sn-glycero-3-phosphocholine (DLPC) fluid membranes (containing one and no unsaturation, respectively), and mapped those values to the corresponding APL according to the calibration carried out using DOPC membranes. Finally, these values were compared to APL values obtained from SAXS/WAXS measurements (Fig. S6).

As seen in Fig. 3b the temperature response (*i.e.* slope) of all fluid membranes was similar, but such relation did not hold for bilayers in the gel phase (Fig. S7). Importantly, we noticed an offset between the model and actual data corresponding to fluid membranes, which could be anticipated from the $\mathcal{P}_0$ term in Eq. 8. However, if a numerical value for this term is obtained either through empirical relations (Fig. S8) or *in-silico* methods, and the membrane composition is not significantly altered during the experiment, Eq. 8 could be used to derive changes in the membrane's structural parameters under stress, by using molecular rotor's fluorescent readout.

This approach would be applicable within timescales where the membrane composition does not vary significantly (e.g. below hour-scale range[11,38]), and it could enable the mapping of the bilayer's structural properties in physiological-relevant setups, which to the best of our knowledge has not been possible using existing techniques.

Combined XRD/FLIM characterization of ternary lipid mixtures reveals the relationship between structure and viscosity in phase-separated membranes: After demonstrating the ability of BC10 MR to indirectly report on the membrane's structural parameters, we increased the complexity of our model membranes by combining DOPC, DPPC and cholesterol (Chol) lipids. This mixture is known to exhibit microscopic phase separation between DOPC rich liquid disordered (L_d) domains and DPPC/Chol rich liquid ordered (L_o) domains,[39] and has been used as a model system of the membrane heterogeneity suspected to occur in cellular membranes.

We electroformed 40:40:20 (%mol) DOPC:DPPC:Chol giant unilamellar vesicles (GUVs) and measured the lifetime of BC10 within the membrane. FLIM imaging, Fig. 4b, revealed two distinct

regions (L_d and L_o) with viscosities of 197±33 cP and 413±128 cP, respectively, in agreement with previous reports.[20] L_d/L_o phase separation was further confirmed by two clearly defined peaks in the SAXS region (Fig. 4c) which correspond to membrane thicknesses of 40.5±0.6 Å and 46.1±0.2 Å for the L_d and L_o phases, respectively. These distinct values for the two phases are consistent with those previously reported[40–42] and exemplify how hydrophobic mismatch is a driving force for lipid phase separation. In addition, these (η, d_{HH}) data pairs show reasonable correlation with those observed in pure DOPC membranes (39.9 Å, 166 cP @20°C) and DPPC bilayers (41.28 Å, 510 cP @30°C). The higher bilayer thickness of DPPC-rich L_o regions can be attributed to the presence of cholesterol, which disrupts the lipid tilt.[43]

Although the presence of two phases was evident in the SAXS region, they could not be clearly resolved from the WAXS diffraction pattern (Fig. 4d), thus preventing an accurate estimation of the lipid-lipid distance. Previous work suggested a 40:40:20 DOPC:DPPC:Chol membrane will contain a relative fraction of cholesterol in the L_d and L_o phase of ~0.1 and 0.3, respectively.[44] Therefore we decided to map the measured lifetimes in GUVs onto calibrations performed on pure DOPC and DPPC/Chol (70/30 %mol) model membranes, Fig. 4e, to obtain an estimate of the APL in the different phases. Our results suggested an area per lipid of 68.3 $Å^2$ and 52.4 $Å^2$ for the L_d and L_o phase, respectively, in good agreement with previous reports (~67$Å^2$ and 52 $Å^2$ for L_d and L_o regions).[42,44,45]

Overall, these results highlight the combination of viscosity-sensitive MRs and FLIM has the potential to be a proxy reporter of the membrane's structure, including those displaying phase-separation.

Line-active molecules disrupt the structural-mechanical relationship of canonical membranes: We finally explored whether our approach could be applied when the hydrophobic height mismatch between the two lipid domains was minimized. This condition has been postulated to be responsible of the transient nature of cellular lipid "rafts",[27,46] and we aimed to mimic it by incorporating line-active molecules, which accumulate at the domain boundary reducing the line tension and the difference in membrane thickness.[47]

An example of such a molecule is oleic acid (OA). Evidence from epidemiological studies suggests that a higher proportion of monounsaturated fatty acids, such as OA, in the diet is linked with a reduction in the risk of coronary heart disease, which is possibly achieved through modification of lipid membrane composition.[48] In this case, OA is known to increase the membrane curvature, thickness and bending rigidity,[49] while the effect on membrane order remains controversial.[50,51] In addition, OA acts as a lineactant,[52] reducing the line tension between L_d and L_o domains, and is thus able to modulate the lateral organization of phase-separated membranes, such as biologically-relevant "lipid rafts".[48,52]

Initially, we investigated the effect of OA in pure DOPC membranes, as they both have the same cis-monounsaturated hydrocarbon chain. The addition of the fatty acid resulted in shift of the SAXS spectra to lower q-values, Fig. S9a,b, indicative of thicker membranes – from 39.3±0.1Å to 46.1±0.2Å – up to 40%mol OA,[50] beyond where the highly curvature imposed by the fatty acid led to the appearance of an inverted hexagonal (H_{II}) phase, as described by *Tyler et al.*[49] and others.[53,54] However, changes in the in-plane membrane distribution were minimal, as judged from the WAXS traces (Fig. S9c,d). On the contrary, the addition of OA lead to an increase of the membrane's bending rigidity[49] and order.[50,55,56] Such reports were consistent with our BC10 measurements indicating an increase in membrane microviscosity from 185±12 cP to 222±25 cP after 40% DOPC was replaced with OA. This

295 change in viscosity corresponded to a decrease in the average APL of -0.24 Å^2 using the calibration
296 depicted in Fig.3b, which was within the same order of magnitude as the one measured directly from
297 the WAXS traces, -0.41 Å^2.

298 Based on this outcome, we then replaced DOPC with OA in phase separated membranes, as OA has
299 a high affinity towards the L_d phase,[52] to investigate whether the disruptive effect of this fatty acid was
300 also observed in ternary lipid mixtures. As a result, we observed an increase in the lattice parameter
301 and membrane thickness of the L_d phase, which saturated at d_{HH} ~45.4 Å for OA concentrations above
302 20%, coupled to a slight decrease in thickness of the L_o domains (Fig. 5b, Fig. S10a,b). At this point, the
303 signals from the L_d and L_o phases appeared to merge in the SAXS pattern, as evidenced by the presence
304 of a single peak at 20% OA. Yet, our microscopy images clearly indicated the presence of distinct lipid
305 domains (Fig. 3c,d), in agreement with previous work by *Shimokawa et al.*[52] This suggests the addition
306 of OA disrupted the structure-viscosity relationship typical of phase separated membranes, thus
307 further reinforcing the idea of the bilayer microviscosity being dictated not only by the membrane's
308 structure but also by the lipid composition itself.

309 Using FLIM measurements of **BC10**, it was clear that the membrane's lateral organization was
310 altered when DOPC was replaced with OA. In particular, adding OA at a 20% molar concentration to
311 replace DOPC led to a change in the GUV morphology, where the total area corresponding to
312 disordered regions decreased and appeared as multiple circular domains within a more ordered matrix
313 (Fig. S11). The lower degree of domain coalescence was likely a consequence of a reduced line tension
314 at the domain's boundary, in agreement with the lower height mismatch between domains when OA
315 was added.[52] In addition, our quantitative analysis (see ESI for details) of lifetime clusters in FLIM
316 images (Fig. 3d & Fig. S12) revealed the presence of three distinct regions of different viscosity
317 (~155±30, ~250±45, ~465±75 cP), which could also be distinguished using a polarity sensitive dye
318 Laurdan[12] (Fig. S13). We also estimated the APL for these regions from the BC10 readings, obtaining
319 approximate values of 68.6, 67.9 and 51.9 Å^2, respectively.

320 Altogether, these findings lead us to hypothesize the domain composition of OA-enriched GUVs
321 could involve the following:

322 (i) *High viscosity* regions (η~465 cP): The membrane thickness and viscosity are similar to OA-
323 free L_o domains, suggesting the relative DPPC:Chol ratio remains unchanged, and OA does
324 not partition significantly into these regions. The estimated APL (51.9 Å^2) is also similar to
325 that of the L_o region in OA-free GUVs.

326 (ii) *Low viscosity* regions (η~155 cP): These are likely domains which predominantly contain
327 DOPC lipids.

328 (iii) *Intermediate viscosity* regions (η~250 cP): The viscosity values are similar to OA-saturated
329 DOPC membranes (Fig. S14), while the membrane thickness is compatible to that of OA-free
330 L_o domains, suggesting this region is rich in DOPC and OA. Remarkably, the ~0.9% decrease
331 in the estimated APL with respect to the low viscosity regions is similar to previous OA-
332 induced changes in the lipid area.[50]

333 Overall, these results suggest microscopic lipid phase separation is possible despite the presence
334 of a height mismatch between the different domains, contrary to the common hypothesis. This
335 situation was previously described by *Mills et al.*, who proposed to use peak splitting in the SAXS region
336 as a sufficient, but not necessary, condition for phase coexistence.[57] Such occurrence could arise, for
337 example, when two domains of different thickness are present if they are unregistered. We note this
338 is not likely the case here, as the increase in membrane thickness of DOPC membranes upon OA

addition is comparable to the value seen in the L_o phase (Fig. S9), thus reinforcing the hypothesis height mismatch suppression in the presence of OA.

CONCLUSIONS

The combination of small and wide-angle X-Ray scattering and FLIM imaging of MRs described here has enabled a combined structural and micromechanical characterization of lipid membranes exhibiting different lipid phases and lateral organization. We demonstrate how the calibration of the fluorescence readout of a molecular probe against known structural descriptors of the membrane allow to use fluorescent dyes to derive quantitative information regarding the molecular organization of the lipid bilayer (e.g. the area per lipid), for both single-component membranes and bilayers containing multiple domains. Finally, we exploited this strategy to demonstrate how the addition of lineactant molecules led to lipid phase separation can occur without hydrophobic mismatch, the most agreed driving force for domain formation. Such lipid arrangements may be of importance in biology, where the lack of hydrophobic mismatch can facilitate the formation of transient lipid nanodomains with distinct mechanical properties ("rafts") while still capable of undergoing easy lipid exchange.

Overall, our approach expands the capability of environmentally sensitive membrane dyes, allowing the estimation of the membrane's structural properties in physio-logically relevant settings. Hence, our approach has the potential to help bridge the gap in the understanding of lateral structuring between model and biological membranes.

REFERENCES

1. Harayama, T. & Riezman, H. Understanding the diversity of membrane lipid composition. *Nat. Rev. Mol. Cell Biol.* **19**, 281–296 (2018).
2. Rawicz, W., Olbrich, K. C., Mcintosh, T., Needham, D. & Evans, E. Effect of Chain Length and Unsaturation on Elasticity of Lipid Bilayers. *Biophys. J.* **79**, 328–339 (2000).
3. Ces, O. & Mulet, X. Physical coupling between lipids and proteins : a paradigm for cellular control. *Signal Transduct.* **6**, 112–132 (2006).
4. Kučerka, N., Heberle, F. A., Pan, J. & Katsaras, J. Structural significance of lipid diversity as studied by small angle neutron and X-ray scattering. *Membranes (Basel).* **5**, 454–472 (2015).
5. Schmid, F. Physical mechanisms of micro- and nanodomain formation in multicomponent lipid membranes. *Biochim. Biophys. Acta - Biomembr.* **1859**, 509–528 (2017).
6. Almeida, P. F. F., Pokorny, A. & Hinderliter, A. Thermodynamics of membrane domains. *Biochim. Biophys. Acta - Biomembr.* **1720**, 1–13 (2005).
7. Lingwood, D. & Simons, K. Lipid rafts as a membrane-organizing principle. *Science (80-.).* **327**, 46–50 (2010).
8. Simons, K. & Toomre, D. Lipid rafts and signal transduction. *Nat. Rev. Mol. Cell Biol.* **1**, 31–39 (2000).
9. Klymchenko, A. S. & Kreder, R. Fluorescent Probes for Lipid Rafts: From Model Membranes to Living Cells. *Chem. Biol.* **21**, 97–113 (2014).
10. Yamamoto, K. & Ando, J. Endothelial cell and model membranes respond to shear stress by

379 rapidly decreasing the order of their lipid phases. *J. Cell Sci.* **126**, 1227–1234 (2013).
380 11. Shimolina, L. E. *et al.* Mapping cisplatin-induced viscosity alterations in cancer cells using
381 molecular rotor and fluorescence lifetime imaging microscopy. *J. Biomed. Opt.* **25**, 1–16 (2020).
382 12. Gunther, G., Malacrida, L., Jameson, D. M., Gratton, E. & Sánchez, S. A. LAURDAN since Weber:
383 The Quest for Visualizing Membrane Heterogeneity. *Acc. Chem. Res.* **54**, 976–987 (2021).
384 13. Colom, A. *et al.* A fluorescent membrane tension probe. *Nat. Chem.* 1–22 (2018).
385 doi:10.1038/s41557-018-0127-3
386 14. Goujon, A. *et al.* Mechanosensitive Fluorescent Probes to Image Membrane Tension in
387 Mitochondria, Endoplasmic Reticulum, and Lysosomes. *J. Am. Chem. Soc.* **141**, 3380–3384
388 (2019).
389 15. Kuimova, M. K. Mapping viscosity in cells using molecular rotors. *Phys. Chem. Chem. Phys.* **14**,
390 12671–12686 (2012).
391 16. García-Calvo, J. *et al.* HydroFlipper membrane tension probes: imaging membrane hydration
392 and mechanical compression simultaneously in living cells. *Chem. Sci.* **13**, 2086–2093 (2022).
393 17. Mahecic, D. *et al.* Mitochondrial membrane tension governs fission. *Cell Rep.* **35**, (2021).
394 18. Hosny, N. A. *et al.* Mapping microbubble viscosity using fluorescence lifetime imaging of
395 molecular rotors. *Proc. Natl. Acad. Sci. U. S. A.* **110**, 9225–9230 (2013).
396 19. Vyšniauskas, A. *et al.* Exploring viscosity, polarity and temperature sensitivity of BODIPY-based
397 molecular rotors. *Phys. Chem. Chem. Phys.* **19**, 25252–25259 (2017).
398 20. Dent, M. R. *et al.* Imaging phase separation in model lipid membranes through the use of
399 BODIPY based molecular rotors. *Phys. Chem. Chem. Phys.* **17**, 18393–18402 (2015).
400 21. Wu, Y. *et al.* Molecular rheometry: direct determination of viscosity in Lo and Ld lipid phases
401 via fluorescence lifetime imaging. *Phys. Chem. Chem. Phys.* **15**, 14986 (2013).
402 22. Páez-Pérez, M., López-Duarte, I., Vyšniauskas, A., Brooks, N. J. & Kuimova, M. K. Imaging non-
403 classical mechanical responses of lipid membranes using molecular rotors. *Chem. Sci.* **12**, 2604–
404 2613 (2021).
405 23. López-Duarte, I., Vu, T. T., Izquierdo, M. A., Bull, J. A. & Kuimova, M. K. A molecular rotor for
406 measuring viscosity in plasma membranes of live cells. *Chem. Commun.* **50**, 5282–5284 (2014).
407 24. Chambers, J. E. *et al.* An Optical Technique for Mapping Microviscosity Dynamics in Cellular
408 Organelles. *ACS Nano* **12**, 4398–4407 (2018).
409 25. Kuimova, M. K., Yahioglu, G., Levitt, J. A. & Suhling, K. Molecular rotor measures viscosity of live
410 cells via fluorescence lifetime imaging. *J. Am. Chem. Soc.* **130**, 6672–6673 (2008).
411 26. Vyšniauskas, A., Qurashi, M. & Kuimova, M. K. A Molecular Rotor that Measures Dynamic
412 Changes of Lipid Bilayer Viscosity Caused by Oxidative Stress. *Chem. - A Eur. J.* **22**, 13210–13217
413 (2016).
414 27. Levental, I., Levental, K. R. & Heberle, F. A. Lipid Rafts: Controversies Resolved, Mysteries
415 Remain. *Trends Cell Biol.* **30**, 341–353 (2020).
416 28. Mills, T. T. *et al.* Liquid-liquid domains in bilayers detected by wide angle x-ray scattering.
417 *Biophys. J.* **95**, 682–690 (2008).
418 29. Hosny, N. A. *et al.* Direct imaging of changes in aerosol particle viscosity upon hydration and
419 chemical aging. *Chem. Sci.* **7**, 1357–1367 (2016).
420 30. Smith, A. J. *et al.* I22: SAXS/WAXS beamline at Diamond Light Source – an overview of 10 years

operation. *J. Synchrotron Radiat.* **28**, 939–947 (2021).

31. Pan, J., Tristram-Nagle, S., Kučerka, N. & Nagle, J. F. Temperature dependence of structure, bending rigidity, and bilayer interactions of dioleoylphosphatidylcholine bilayers. *Biophys. J.* **94**, 117–124 (2008).

32. Eicher, B. *et al.* Intrinsic Curvature-Mediated Transbilayer Coupling in Asymmetric Lipid Vesicles. *Biophys. J.* **114**, 146–157 (2018).

33. Jadidi, T., Seyyed-Allaei, H., Tabar, M. R. R. & Mashaghi, A. Poisson's ratio and Young's modulus of lipid bilayers in different phases. *Front. Bioeng. Biotechnol.* **2**, 1–6 (2014).

34. Parasassi, T., Krasnowska, E. K., Bagatolli, L. & Gratton, E. Laurdan and Prodan as Polarity-Sensitive Fluorescent Membrane Probes. *J. Fluoresc.* **8**, 365–373 (1998).

35. Ma, Y., Benda, A., Kwiatek, J., Owen, D. M. & Gaus, K. Time-Resolved Laurdan Fluorescence Reveals Insights into Membrane Viscosity and Hydration Levels. *Biophys. J.* 1–11 (2018). doi:10.1016/j.bpj.2018.08.041

36. Leung, S. S. W., Brewer, J., Bagatolli, L. A. & Thewalt, J. L. Measuring molecular order for lipid membrane phase studies: Linear relationship between Laurdan generalized polarization and deuterium NMR order parameter. *Biochim. Biophys. Acta - Biomembr.* **1861**, 183053 (2019).

37. Sun, W. J., Tristram-Nagle, S., Suter, R. M. & Nagle, J. F. Structure of gel phase saturated lecithin bilayers: Temperature and chain length dependence. *Biophys. J.* **71**, 885–891 (1996).

38. Budin, I. *et al.* Viscous control of cellular respiration by membrane lipid composition. *Science (80-.).* **362**, 1186–1189 (2018).

39. Veatch, S. L. & Keller, S. L. Separation of Liquid Phases in Giant Vesicles of Ternary Mixtures of Phospholipids and Cholesterol. *Biophys. J.* **85**, 3074–3083 (2003).

40. Barriga, H. M. G., Law, R. V., Seddon, J. M., Ces, O. & Brooks, N. J. The effect of hydrostatic pressure on model membrane domain composition and lateral compressibility. *Phys. Chem. Chem. Phys.* **18**, 149–155 (2016).

41. Chen, L., Yu, Z. & Quinn, P. J. The partition of cholesterol between ordered and fluid bilayers of phosphatidylcholine: A synchrotron X-ray diffraction study. *Biochim. Biophys. Acta - Biomembr.* **1768**, 2873–2881 (2007).

42. Wang, Y., Gkeka, P., Fuchs, J. E., Liedl, K. R. & Cournia, Z. DPPC-cholesterol phase diagram using coarse-grained Molecular Dynamics simulations. *Biochim. Biophys. Acta - Biomembr.* **1858**, 2846–2857 (2016).

43. Alavizargar, A., Keller, F., Wedlich-Söldner, R. & Heuer, A. Effect of Cholesterol Versus Ergosterol on DPPC Bilayer Properties: Insights from Atomistic Simulations. *J. Phys. Chem. B* **125**, 7679–7690 (2021).

44. Ma, Y. *et al.* Cholesterol Partition and Condensing Effect in Phase-Separated Ternary Mixture Lipid Multilayers. *Biophys. J.* **110**, 1355–1366 (2016).

45. Smondyrev, A. M. & Berkowitz, M. L. Structure of dipalmitoylphosphatidylcholine/cholesterol bilayer at low and high cholesterol concentrations: Molecular dynamics simulation. *Biophys. J.* **77**, 2075–2089 (1999).

46. Veatch, S. L. & Cicuta, P. Critical lipidomics: The consequences of lipid miscibility in biological membranes. *Phys. Biol. Membr.* 141–168 (2018). doi:10.1007/978-3-030-00630-3_6

47. Brewster, R. & Safran, S. A. Line active hybrid lipids determine domain size in phase separation

of saturated and unsaturated lipids. *Biophys. J.* **98**, L21–L23 (2010).

48. Lopez, S. *et al.* Membrane composition and dynamics: A target of bioactive virgin olive oil constituents. *Biochim. Biophys. Acta - Biomembr.* **1838**, 1638–1656 (2014).

49. Tyler, A. I. I., Greenfield, J. L., Seddon, J. M., Brooks, N. J. & Purushothaman, S. Coupling phase behavior of fatty acid containing membranes to membrane bio-mechanics. *Front. Cell Dev. Biol.* **7**, 1–10 (2019).

50. Leekumjorn, S. *et al.* The role of fatty acid unsaturation in minimizing biophysical changes on the structure and local effects of bilayer membranes. *Biochim. Biophys. Acta - Biomembr.* **1788**, 1508–1516 (2009).

51. Jacobs, M. L., Faizi, H. A., Peruzzi, J. A., Vlahovska, P. M. & Kamat, N. P. EPA and DHA differentially modulate membrane elasticity in the presence of cholesterol. *Biophys. J.* **120**, 2317–2329 (2021).

52. Shimokawa, N., Mukai, R., Nagata, M. & Takagi, M. Formation of modulated phases and domain rigidification in fatty acid-containing lipid membranes. *Phys. Chem. Chem. Phys.* **19**, 13252–13263 (2017).

53. Gillams, R. J., Nylander, T., Plivelic, T. S., Dymond, M. K. & Attard, G. S. Formation of inverse topology lyotropic phases in dioleoylphosphatidylcholine/oleic acid and dioleoylphosphatidylethanolamine/ oleic acid binary mixtures. *Langmuir* **30**, 3337–3344 (2014).

54. Funari, S. S., Barceló, F. & Escribá, P. V. Effects of oleic acid and its congeners, elaidic and stearic acids, on the structural properties of phosphatidylethanolamine membranes. *J. Lipid Res.* **44**, 567–575 (2003).

55. Franz, J. *et al.* Nitrated Fatty Acids Modulate the Physical Properties of Model Membranes and the Structure of Transmembrane Proteins. *Chem. - A Eur. J.* **23**, 9690–9697 (2017).

56. De Santis, A. *et al.* Omega-3 polyunsaturated fatty acids do not fluidify bilayers in the liquid-crystalline state. *Sci. Rep.* **8**, 1–13 (2018).

57. Mills, T., Huang, J., Feigenson, G. & Nagle, J. Effects of cholesterol and unsaturated DOPC lipid on chain packing of saturated gel-phase DPPC bilayers. *Gen. Physiol. Biophys.* **28**, 126–139 (2009).

Acknowledgements

MPP acknowledges the Engineering and Physical Sciences Research Council (EPSRC) and the British Heart Foundation (BHF) for the Doctoral Training Studentship (EP/L015498/1, RE/13/4/30184) from the Institute of Chemical Biology (Imperial College London). MKK. is grateful to the EPSRC for a Career Acceleration Fellowship (EP/I003983/1). This work was carried out with the support of Diamond Light Source, instrument I22 (proposals SM28072 and SM29165).

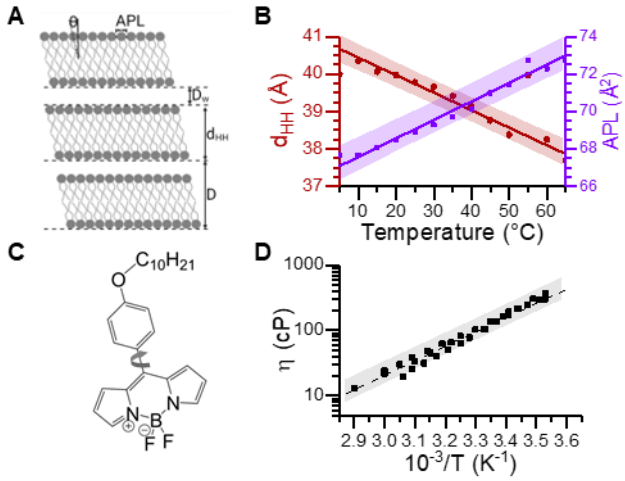

Figure 1. The effect of temperature on the lipid membrane structure and viscosity. (A) The structural parameters APL, tilt angle (Θ), dHH, water layer thickness (D_W) and lamellar repeat spacing (D) are extracted from SAXS and WAXS diffraction patterns. (B) Increasing the temperature leads to a higher degree of chain splay, which commonly results in a decrease of d_{HH} and an increase of the APL. (C) Structure of MR BC10. (D) Andrade's relationship between membrane viscosity and temperature in DOPC membranes.

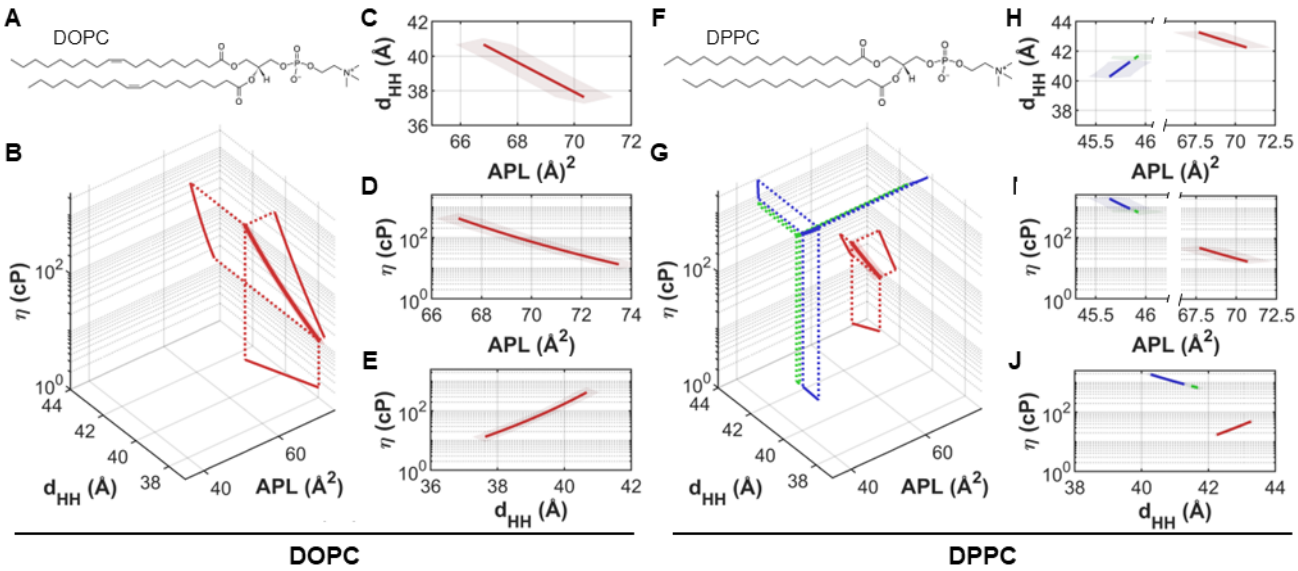

Figure 2. The relationship between the membrane's structural and mechanical properties as a function of the lipid phase. (A,F) Molecular structure of DOPC and DPPC. (B,G) 3D plots showing the interrelations between d_{HH}, APL and η, as measured by MR BC10. Corresponding 2D projections of the 3D plots: (C,H) d_{HH} vs APL plots, from which the Poisson ratio ν can be extracted. (D,I) Relationship between η and APL. (E,J) Influence of d_{HH} on η. Colour coding corresponds to tilted gel $L_{\beta'}$ (blue), ripple $P_{\beta'}$ (green) and fluid L_{α} (red) lipid phase.

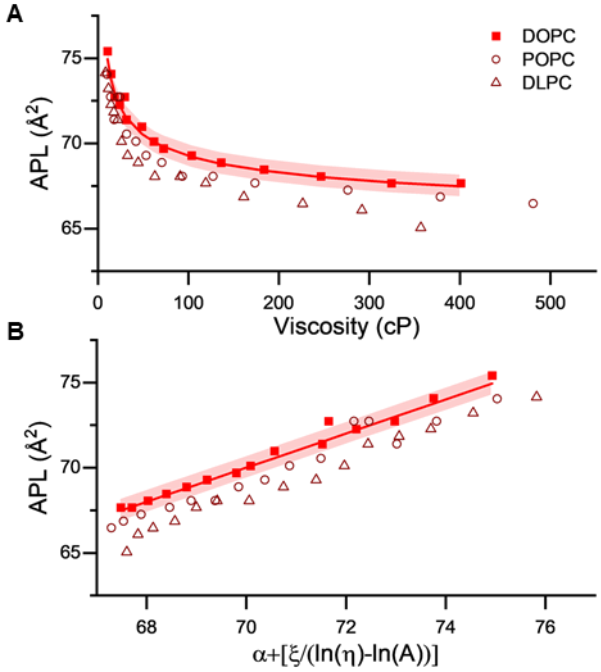

Figure 3. Membrane's viscosity-structure relationship is maintained in fluid lipid bilayers. (A) Relationship between microviscosity reported by BC10. (B) Relationship between APL and the transformed viscosity according to Eq. 8, showing the lipid-dependent offset.

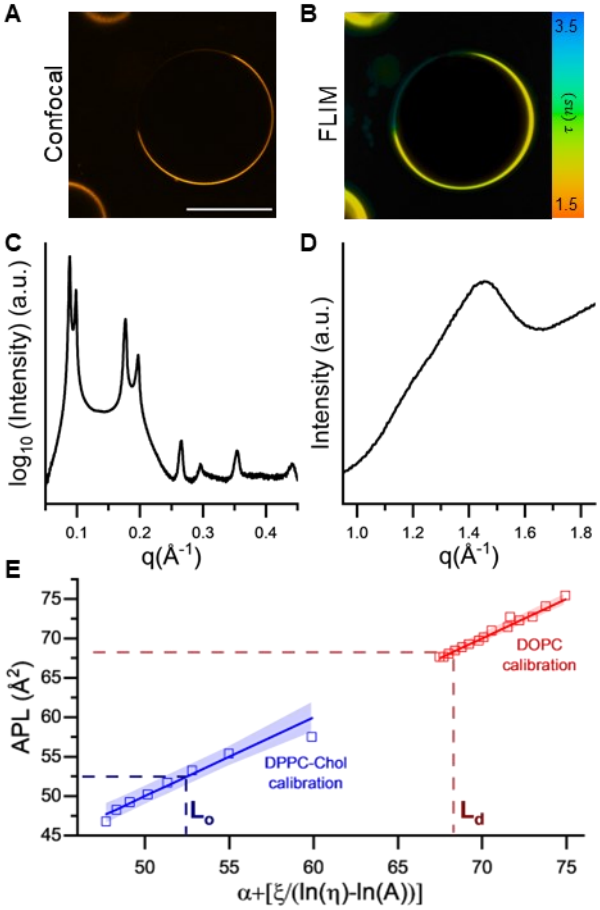

Figure 4. MRs can be used to infer structural properties of membrane domains. (A) Confocal and (B) FLIM images of 40:40:40 DOPC:DPPC:Chol GUVs. Scalebar: 30µm. (C) SAXS and (D) WAXS traces corresponding to the lipid mixture used in (A). While bilayer thickness can be easily extracted from the clearly-defined SAXS peaks, estimation of the APL from the WAXS pattern is challenging. (E) Calibration in known lipid mixtures allows to estimate the APL in the L_d and L_o phases.

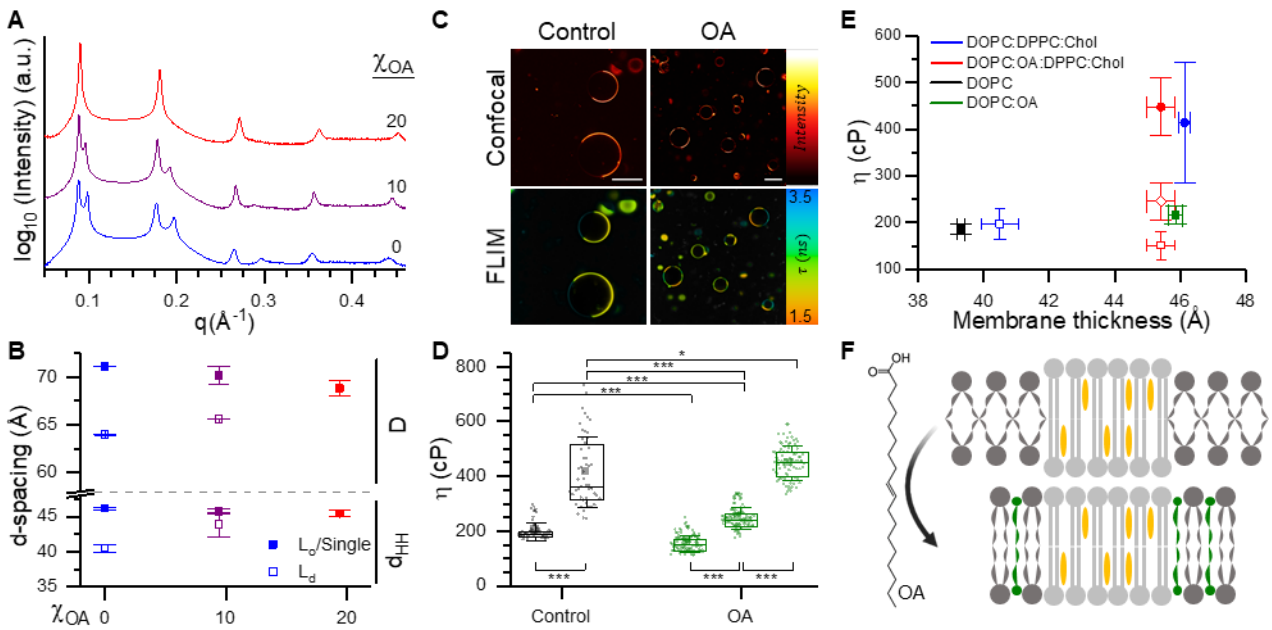

Fig. 5 The effect of oleic acid (OA) on phase separation. (A) SAXS pattern from DOPC:OA:DPPC:Chol membranes with increasing OA replacing DOPC . (B) Effect of increasing OA on lamellar repeat spacing and membrane thickness. (C) Confocal and FLIM micrographs of 40:0:40:40 and 20:20:40:20 DOPC:OA:DPPC:Chol GUVs. Scalebar: 30µm. (D) Box plot showing the change in viscosity upon OA addition. (E) Plot of membrane viscosity against membrane thickness. (F) Schematic showing a possible interaction of OA with phase separated membranes.